Available online at www.sciencedirect.com
ScienceDirect
Solid State Communications 141 (2007) 127–131
solid state communications
www.elsevier.com/locate/ssc

# Mechanisms of femtosecond laser-induced damage in magnesium fluoride

Haiyi Sun[a,*], Tianqing Jia[a,b], Chengbin Li[a], Xiaoxi Li[a], Shizhen Xu[a], Donghai Feng[a], Xiaofeng Wang[a], Xiaochun Ge[a], Zhizhan Xu[a]

[a] *State Key Laboratory of High Field Laser Physics, Shanghai Institute of Optics and Fine Mechanics, Chinese Academy of Sciences, Shanghai 201800, China*
[b] *The Institute for Solid State Physics, The University of Tokyo, 5-1-5 Kashiwanoha, Kashiwa, Chiba 277-8581, Japan*

Received 10 May 2006; received in revised form 21 July 2006; accepted 13 October 2006 by R. Phillips
Available online 30 October 2006

**Abstract**

We studied the single-shot damage in magnesium fluoride irradiated by 800 nm femtosecond (fs) laser. The dependence of damage thresholds on the laser pulse durations from 60 to 750 fs was measured. The pump–probe measurements were carried out to investigate the time-resolved electronic excitation processes. A coupled dynamic model was applied to study the microprocesses in the interaction between fs laser and magnesium fluoride. The results indicate that both multiphoton ionization and avalanche ionization play important roles in the femtosecond laser-induced damage in $MgF_2$.


*PACS:* 77.84.-s; 72.20.Ht; 78.47.+p; 82.40. Js

*Keywords:* A. Magnesium fluoride; D. Damage mechanisms; E. Femtosecond laser; E. Pump–probe measurements

## 1. Introduction

Femtosecond laser-induced damage in transparent dielectrics has been studied extensively [1–5], and it is a complex ultrafast dynamic process including electron excitation and relaxation processes. The pump–probe technique is an effective tool in investigating the ultrafast dynamic process. It has already been used in measuring the ultrafast processes of semiconductors, transparent bulk materials, and nanostructure materials irradiated by nanosecond and femtosecond lasers [6–10]. By measuring time-resolved reflectivity, transmissivity and the luminescence spectrum, the ultrafast nonlinear optical response of materials, such as the excitation and the relaxation processes of electron and crystal lattice can be investigated. However, as far as we know, in previous experiments, the durations of the pump and probe pulses were usually equal, and only the relaxation processes were studied intensively [9,10]. The time-resolved excitation processes could not be investigated in detail. Therefore, significant controversies about the electronic excitation processes remain, and the relative role between multiphoton ionization and avalanche ionization in the generation of conduction band electrons (CBE) is far from fully understood [11,12]. In addition, wide-band-gap $MgF_2$ crystals are potential materials as windows, lenses and fiber guides [13]. However, there are only a few reports on the damage of $MgF_2$ [14].

In this paper, we investigated the time-resolved reflectivity in $MgF_2$ crystal by means of a developed pump–probe system, in which the pump pulse was stretched to 750 fs, while the duration of probe pulse was only 60 fs. We also applied a coupled dynamic model to study the single-shot damage mechanisms of $MgF_2$ crystal irradiated by 800 nm fs laser.

## 2. Experimental setup

The experiments were conducted with a chirp pulse amplified Ti: sapphire laser system. Its standard output was 60 fs, 0.6 mJ at a wavelength of 800 nm. In the damage threshold experiment, we changed the pulse energy continuously by a half wave plate and a polarizer, and the pulse duration by a compression grating. The linearly polarized Gaussian laser beam was vertically focused on the front surface of the sample using a 150 mm-focal-length lens. We monitored the sample surface with a microscope objective (NA = 0.1) and a charge-coupled device (CCD). For a given pulse duration, the pulse energy was decreased until the damage spot could not be

* Corresponding author.
*E-mail address:* shy780327@siom.ac.cn (H. Sun).

0038-1098/$ - see front matter © 2006 Elsevier Ltd. All rights reserved.
doi:10.1016/j.ssc.2006.10.012

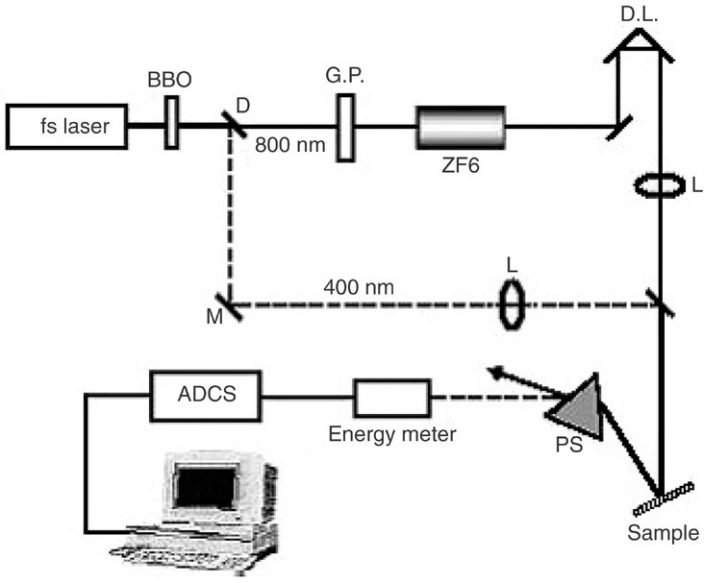


Fig. 1. Schematic setup for pump–probe experiment. D: dichroic mirror, G.P.: Glan prism, D.L.: delay line, M: 400 nm high-reflection mirror, L: lens, ADCS: automatic data acquisition system, PS: prism.

observed through the CCD. After irradiation, the spot area and the morphology were measured with a higher-resolution optical microscope (NA = 0.65) and a scanning electronic microscope (SEM), respectively. Based on the relation between the spot areas and the laser fluences, we could calculate the damage threshold for every pulse duration.

The pump–probe experimental setup has been described in detail elsewhere [15], and only a brief description is given here (Fig. 1). The 800 nm laser pulse propagated through a BBO crystal and underwent frequency doubling. It was then split into an 800 nm pump pulse and a 400 nm probe pulse. The pulse duration of pump laser was stretched to 750 fs by means of ZF6 glass, and then it passed through a delay line. The pump and the probe laser pulses were focused by two lenses, and then were collinear and confocal on the front surface of the sample at an incident angle of 10°. The time zero point was determined by measuring the sum-frequency signal of the pump and the probe pulses. The reflected 400 nm s-polarized probe signal passed through a prism, and then was recorded by an energy meter (nJ energy resolution). The energy of the probe pulse was only a few hundred nanojoule (nJ), well below its single-shot damage threshold. In both the damage threshold and the pump–probe experiments, the sample was set on a three-dimensional translation stage to insure each new area on the sample was irradiated by only one laser pulse.

The dimension of the single crystal $MgF_2$ is 10 × 10 × 1 mm. The slab surface is (111). Both large sides are optically polished, and the roughness is less than 10 nm.

## 3. Theory

On the basis of the avalanche model, CBE are generated by photoionization and impact ionization. The evolution equation of CBE density $n_e(t)$ can be written as follows [16]

$$\frac{\partial n_e(t)}{\partial t} = (R_{\mathrm{PI}}(I) + R_{I\!I}(I) \cdot n_e)\left(1 - \frac{n_e(t)}{N_0}\right), \tag{1}$$

where $R_{\mathrm{PI}}$ and $R_{I\!I}$ are the photoionization rate and the impact ionization rate, respectively. $I(t)$ is the incident laser intensity. The factor $1 - \frac{n_e}{N_0}$ is introduced for the consideration of the exhaustion of valence band electrons (VBE). We considered that only one VBE in a molecule was excited to the conduction band, and hence the initial number of VBE ($N_0$) is equal to that of molecules in the material [17]. The initial number of VBE ($N_0$) is $6.5 \times 10^{22}$ cm$^{-3}$.

Photoionization includes both multiphoton ionization (MPI) and tunneling ionization, which can be calculated by Kelsysh theory [18,19]. We calculated the photoionization rate $R_{\mathrm{PI}}$ of the $MgF_2$ crystal as a function of laser intensity $I$ at the wavelength of 800 nm, and found that when the laser intensity was less than 200 TW/cm$^2$, CBE were produced by the MPI process.

The impact ionization $R_{I\!I}$ was calculated using the flux-doubling model [20,21]. It is expressed as

$$R_{I\!I} = 1 \Big/ \int_0^{E_g} \frac{\mathrm{d}E_K}{W(E_K)}, \tag{2}$$

where $E_K$ is CBE kinetic energy, which is almost always in the range of $0 \le E_K \le E_g$ [20]. $W(E_K)$ is the absorption rate of laser energy at $E_K$. We calculated the rate of CBE absorption of laser energy by using standard perturbation theory [22], which includes one-photon and two-photon absorption rates.

The incident laser pulse is a Gaussian pulse with intensity $I(t)$ as [23]

$$I(t) = I_{\max}(t) \exp\left[(-4 \ln 2)\left(\frac{t}{\tau}\right)^2\right], \tag{3}$$

where $I_{\max}$ and $\tau$ are the peak intensity and the pulse duration, respectively.

With increasing CBE density, the plasma has effects on the dielectric function $\varepsilon^*$ and laser intensity distribution in the sample, which in turn affects the production of CBE. The

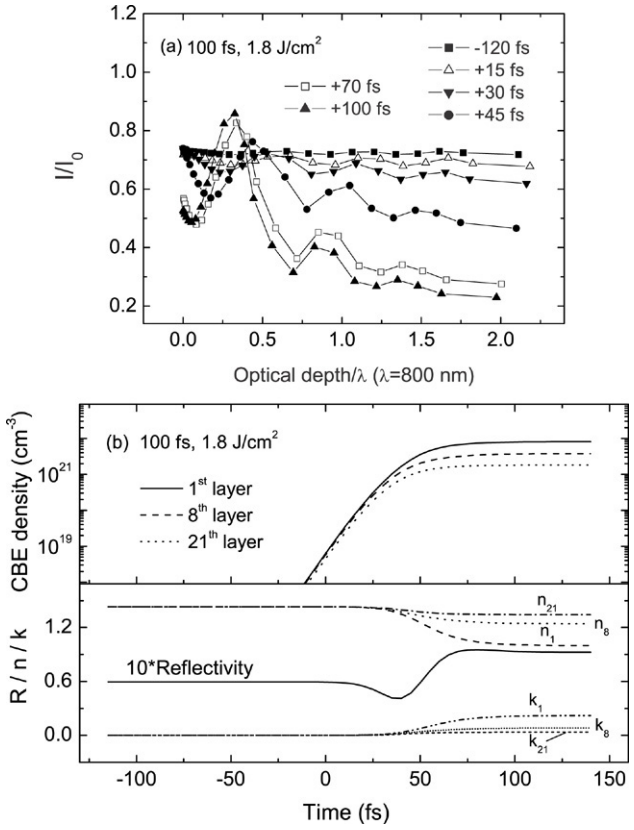


Fig. 2. Calculated evolution of: (a) laser intensity $I/I_0$; (b) CBE density $n_e$, refractive index $n$, and extinction coefficient $k$ in the first, eighth, and twenty-first layer, and reflectivity $R$ of $MgF_2$. The subscripts 1, 8 and 21 denote the first, eighth and twenty-first layer, respectively.

dependence of $\varepsilon^*$ on $n_e(t)$ can be expressed as [24]

$$\varepsilon^*(\hbar\omega) = 1 + [\varepsilon(\hbar\omega) - 1]\frac{N_0 - n_e}{N_0} - \frac{n_e e^2}{\varepsilon_0 m^*_{\text{opt}} m_e \omega^2}\frac{1}{1 + \mathrm{i}\frac{1}{\omega\tau_D}}, \quad (4)$$

where $\varepsilon_0$, $m_e$, $e$ and $\omega$ are the vacuum dielectric constant, free electron mass, electronic charge and laser frequency, respectively. $\varepsilon(\hbar\omega)$ is the dielectric constant of the unexcited material, which is 1.90 at a wavelength of 800 nm and 2.16 − i0.006 at a wavelength of 400 nm. $m^*_{\text{opt}} = (m_e^{*-1} + m_h^{*-1})^{-1}$ represents the optical effective mass of the carriers ($m_e^*$ and $m_h^*$ are the effective masses of electrons and holes, respectively), which was chosen as the free electron mass $m_e$ (=1) [16,24]. The Drude damping time $\tau_D$ of $MgF_2$ was taken as 1 fs [24].

In order to calculate the spatial distribution of laser intensity, we treated the bulk sample as a stack of thin layers [16]. The thickness of each layer is (0.01, 0.02, 0.03, 0.05, 0.07, 0.09, 0.12, 0.15, 0.17, 0.2, 0.25, 0.3, 0.3, 0.3, 0.55, 0.55, 0.55, 0.55, 0.55, 0.55, 0.55, 0.55, 0.6, 1.28) × λ/4$n$, where $n$ is the refractive index at a wavelength λ of 800 nm. First, we adopted the thin-film optics theory [25] to calculate the distribution of laser intensity, and then solved Eq. (1) numerically to study $n_e$ evolution, and further calculated $\varepsilon^*$ by Eq. (4). Hereafter, we recalculated the laser intensity distribution. This recycle was repeated with a time step of 2 fs.

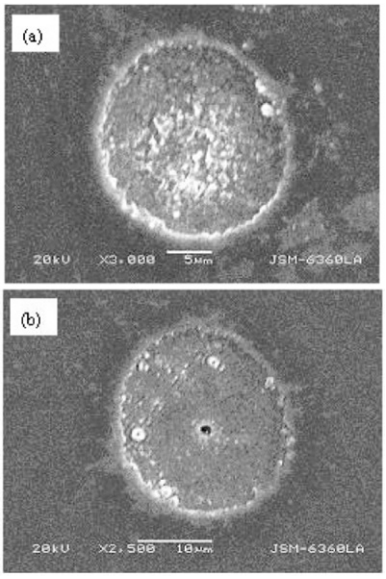


Fig. 3. Damage morphology of $MgF_2$ irradiated by 800 nm laser, (a) $F$ = 6.0 J/cm², $\tau$ = 100 fs; (b) $F$ = 10.2 J/cm², $\tau$ = 60 fs.

The calculation results are presented in Fig. 2. Fig. 2(a) shows the ultrafast evolution of the distribution of laser intensity $I/I_0$, which indicates that the laser intensity distribution is very different from its initial case when the delay time is larger than +45 fs. $I$ and $I_0$ represent the laser intensity in the material and in the air, respectively. Fig. 2(b) shows the evolution of CBE density $n_e$, refractive index $n$, and extinction coefficient $k$ in the first, eighth, and twenty-first layer, and the reflectivity $R$ of $MgF_2$. In our calculation, the parameters of the laser pulse are set as 100 fs pulse width, 800 nm wavelength, and 1.8 J/cm² laser fluence with Gaussian distribution. $n_e$ increases to the order of $10^{20}$ cm$^{-3}$ when the delay time closes to 15 fs, which induces a decrease of $n$ and an increase of $k$. Therefore, the reflectivity $R$ of the sample begins to decrease. When the delay time closes to 35 fs, $n_e$ increases to the order of $10^{21}$ cm$^{-3}$ and $R$ decreases to a minimum. Then, with the quick increase of $n_e$, $R$ also rises quickly. Our theoretical results indicate that the excitation of CBE changes $n$, $k$ and $R$, and further changes the distribution of the laser intensity. The changed distribution of laser intensity inversely influence the production of CBE.

## 4. Results and discussion

### 4.1. Ablation morphology

Fig. 3(a) and (b) show the typical SEM pictures irradiated by femtosecond laser pulse. We can see the clear edge with no evident indication of melting. Shallow ablation is observed at a diameter of less than 20 μm under smaller laser intensity (Fig. 3(a)). When the laser intensity increases, a small hole in the center (diameter 1–2 μm) appears (Fig. 3(b)). Therefore, machining higher quality and smaller holes can be realized in $MgF_2$ by means of femtosecond laser.

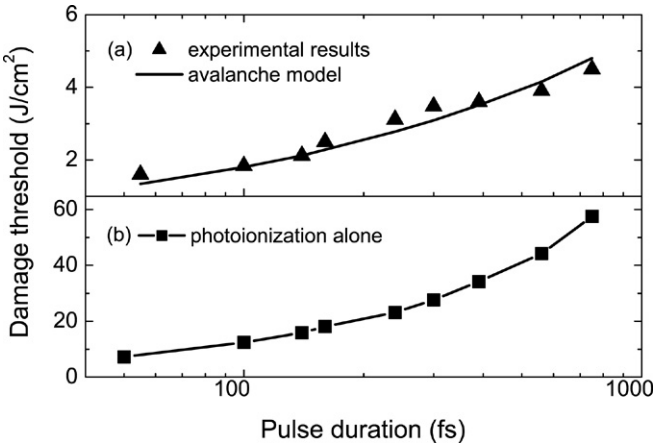


Fig. 4. Measured and calculated damage thresholds as a function of pulse durations. The solid triangles in (a) show the experimental results. The solid line in (a) and the squares in (b) indicate the avalanche and the photoionization alone fitting results, respectively.

### 4.2. Ablation threshold

We measured the damage spot areas with an optical microscope. According to the linear relationship between the ablated area and the laser energy, we obtained the dependence of damage threshold on the laser pulse duration [14,26]. The triangles in Fig. 4 show the experimental results. With decreasing the pulse duration from 750 to 60 fs, the damage thresholds vary from 4.5 to 1.6 J/cm$^2$.

The solid line in Fig. 4(a) shows the calculated laser-induced damage threshold in magnesium fluoride. Here we think the sample is damaged when the CBE density increases to a critical density $N_{\text{crit}}$ of $3.817 \times 10^{21}$ cm$^{-3}$, which is determined by the free-electron density of plasma resonance absorption [24,27,28]. In the photoionization simulating (Fig. 4(b)), the impact ionization rate in Eq. (1) was taken as zero. From the fitting results, we can conclude that the avalanche theory well explains the experimental results, while the photoionization simulation deviates greatly. The results indicate that CBE in $MgF_2$ crystal are produced by both multiphoton ionization and impact ionization.

### 4.3. Time-resolved reflectivity

Fig. 5(a) and (b) show the experimental results for time-resolved reflectivity under the excitation of different pump fluences. The reflectivity and the time zero point were measured six times. Fig. 5(b) is the magnification of the excitation process. The wavelength of pump pulse was 800 nm with 750 fs pulse duration. The probe pulse had a wavelength of 400 nm with 60 fs pulse duration. The increase of reflectivity during the pump laser irradiation is attributed to high-density plasma [24]. When the pump pulse intensity is 5.8 J/cm$^2$, the reflectivity of the probe beam starts to increase as the delay time $t = 200$ fs, and goes up rapidly at the latter half of the pump pulse. With increasing pump intensity to 7.7 J/cm$^2$, the start point advances to about 0 fs, but the reflectivity still increases rapidly at the latter half of the pump pulse. Our experimental results do not support the proposal that MPI plays

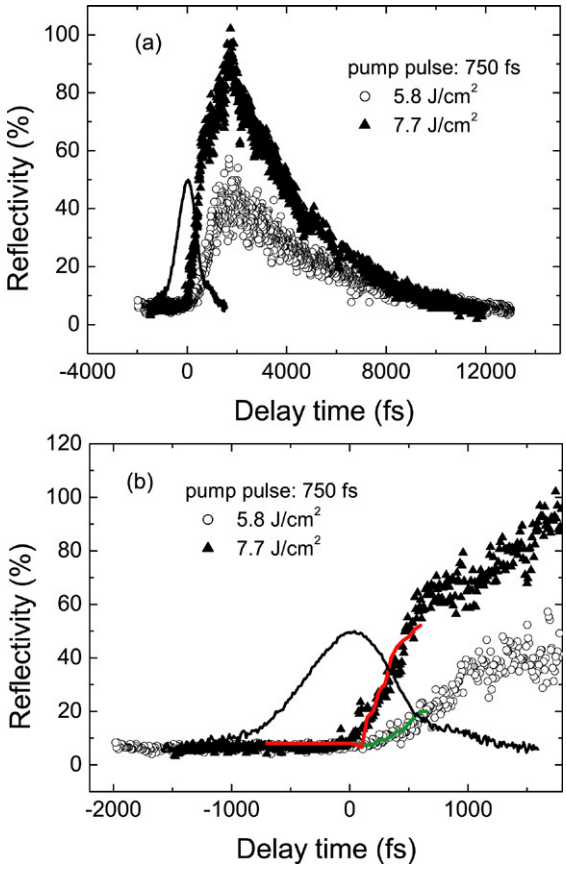


Fig. 5. (a) Time-resolved reflectivity of 400 nm probe pulse under the irradiation of 800 nm pump pulse with pulse fluences of 5.8 and 7.7 J/cm$^2$. (b) Magnification of the excitation process. The Gaussian solid lines in (a) and (b) show the pump pulses. The red and the green lines in (b) are our calculation results. (For interpretation of the references to colour in this figure legend, the reader is referred to the web version of this article.)

the dominant role in femtosecond laser-induced damage in dielectrics. The band gap of the $MgF_2$ crystal is 11.8 eV [5], while the photonic energy of the 800 nm laser is 1.55 eV. Therefore, a valence electron will absorb 7 photons when it is excited into the conduction band via MPI. The MPI rate $R_{\text{MPI}} \propto I^7$. If MPI plays the dominant role in CBE production, the reflectivity should increase rapidly at the peak rather than in the latter half of the pump pulse. The experimental results in Fig. 5 can be well explained by the avalanche model [1,2]: MPI provides the initial seed electrons, which triggers impact ionization in the latter half of the pulse and causes the CBE density to increase exponentially. Therefore, our experimental results indicate that CBE in $MgF_2$ crystal are produced by both MPI and impact ionization. The experimental results of time-resolved reflectivity in other wide-band-gap materials, such as MgO [29] and $CaF_2$ [30], also support the same point.

Because of the Gaussian distribution of laser intensity, the reflectivity of probe pulse does not change synchronously. The measured reflectivity by energy meter is a spatial average value. Therefore, using the coupled Eqs. (1)–(4), we calculated the evolution of reflectivity for a 400 nm-wavelength probe beam by weighted averaging of the different irradiation fluences in space ($I_0$, $\frac{1}{2}I_0$, $\frac{1}{4}I_0$, $\frac{1}{8}I_0$, $\frac{1}{16}I_0$), which are shown as the red and

Table 1
The modeling parameters for $MgF_2$

| Parameters | $MgF_2$ |
|---|---|
| $E_g$ (eV) | 11.8 |
| $N_0$ ($10^{22}$ cm$^{-3}$) | 6.5 |
| $m^*_{opt}$ | 1.0 |
| $\tau_D$ (fs) | 1.0 |

the green solid lines in Fig. 5(b). The coupled theory well explains the pump–probe experimental results, which supports the idea that impact ionization plays an important role in CBE production.

The modeling parameters are listed in Table 1. In these parameters, the variation of $m^*_{opt}$ is the most sensitive to the calculations, because it can affect the CBE production directly through MPI, impact ionization and dielectric function. If it increases to $2m_e$, the photoionization rate and the impact ionization rate decrease by ∼92% and 3%–5%, respectively. This will lead to a decrease of CBE density, consequently inducing a change of reflectivity. CBE density in the first layer decreases by two orders of magnitude, and by one order of magnitude in other layers, which results in a ∼90% decrease in probe reflectivity. $E_g$ can affect MPI and impact ionization rates. When $E_g$ varies from 11.8 to 12.8 eV, the photoionization rate and the impact ionization rate decrease by ∼55% and 1%–3%, respectively, which causes the changes of probe reflectivity at the minimum and the maximum, while it has no evident effect on the slope of the rising part. The reflectivity at the minimum decreases by ∼35%, and increases by ∼5% at the maximum. The Drude damping time $\tau_D$ affects the magnitude of the imaginary part of $\varepsilon^*$. When $\tau_D$ increases to 2 fs, the calculated probe reflectivity at the minimum, the maximum, and the rising part increase by about 93%, 17% and 12%, respectively. Furthermore, the locating time of the minimum advances by ∼50 fs. The effect of $N_0$ is determined by the factor $\frac{N_0-n_e}{N_0}$, whose variation is insensitive to the calculation results due to the small magnitude of $\frac{N_0-n_e}{N_0}$ ($<1$). At low laser intensity, this effect is very weak because $\frac{N_0-n_e}{N_0} \ll 1$.

## 5. Conclusions

We studied the single-shot damage mechanisms of $MgF_2$. The damage thresholds increase from 1.6 to 4.5 J/cm$^2$ with pulse durations ranging from 60 to 750 fs. The ultrafast electron dynamics of the excitation process was investigated by our developed pump–probe technique. The reflectivity increases rapidly in the latter half of the pump pulse, rather than at its peak. Considering the interaction between the laser pulse and the dielectric, we established and solved a coupled dynamic model. Using this model, we studied the ultrafast electron excitation and damage mechanisms. The results indicate that CBE in $MgF_2$ crystals are produced by both multiphoton ionization and impact ionization.

## Acknowledgments

This work was supported by the Chinese National Natural Science Foundation (No 60108002) and the Chinese National Major Basic Research Project (No. G1999075200).

## References

[1] D. Du, X. Liu, G. Korn, J. Squier, G. Mourou, Appl. Phys. Lett. 64 (1994) 3071.
[2] B.C. Stuart, M.D. Feit, S. Herman, A.M. Bubenchik, B.W. Shore, M.D. Perry, Phys. Rev. Lett. 74 (1995) 2248.
[3] R. Stoian, A. Rosenfeld, D. Ashkenasi, I.V. Hertel, N.M. Bulgakova, E.E.B. Campbell, Phys. Rev. Lett. 88 (2002) 097603.
[4] A. Kaiser, B. Rethfeld, M. Vicanek, G. Simon, Phys. Rev. B 61 (2000) 11437.
[5] D.M. Simanovskii, H.A. Schwettman, H. Lee, A.J. Welch, Phys. Rev. Lett. 91 (2003) 107601.
[6] P. Audebert, S. Guizard, K. Krastev, P. Martin, G. Petite, A.D. Santos, A. Antonetti, Phys. Rev. Lett. 73 (1994) 1990.
[7] M. Li, S. Menon, J.P. Nibarger, G.N. Gibson, Phys. Rev. Lett. 82 (1999) 2394.
[8] X. Mao, S.S. Mao, R.E. Russo, Appl. Phys. Lett. 82 (2003) 697.
[9] K. Tanimura, Phys. Rev. B 63 (2001) 184303.
[10] R. Lindner, M. Reichling, R.T. Williams, E. Matthias, J. Phys. Condens. Matter 13 (2001) 2339.
[11] F. Quéré, S. Guizard, P. Martin, Europhys. Lett. 56 (2001) 138.
[12] B. Rethfeld, Phys. Rev. Lett. 92 (2004) 187401.
[13] B. Bendow, H.G. Lipson, Phys. Rev. B 20 (1979) 1747.
[14] D. von der Linde, H. Schüler, J. Opt. Soc. Amer. B 13 (1996) 216.
[15] C.B. Li, D.H. Feng, T.Q. Jia, H.Y. Sun, X.X. Li, S.Z. Xu, X.F. Wang, Z.Z. Xu, Solid State Commun. 136 (2005) 389.
[16] T.Q. Jia, H.X. Chen, M. Huang, F.L. Zhao, X.X. Li, S.Z. Xu, H.Y. Sun, D.H. Feng, C.B. Li, X.F. Wang, R.X. Li, Z.Z. Xu, X.K. He, H. Kuroda, Phys. Rev. B 73 (2006) 054105.
[17] T.Q. Jia, Z.Z. Xu, R.X. Li, D.H. Feng, X.X. Li, C.F. Cheng, H.Y. Sun, N.S. Xu, H.Z. Wang, J. Appl. Phys. 95 (2004) 5166.
[18] L.V. Keldysh, Sov. Phys. JETP 20 (1965) 1307.
[19] S.S. Mao, F. Quéré, S. Guizard, X. Mao, R.E. Russo, G. Petite, P. Martin, Appl. Phys. A 79 (2004) 1695.
[20] B.C. Stuart, M.D. Feit, S. Herman, A.M. Rubenchik, B.W. Shore, M.D. Perry, Phys. Rev. B 53 (1996) 1749.
[21] T.Q. Jia, H. Chen, Y.M. Zhang, Phys. Rev. B 61 (2000) 16522.
[22] T.Q. Jia, R.X. Li, Z. Liu, Z.Z. Xu, Appl. Phys. A 74 (2002) 503.
[23] C.H. Fan, J. Sun, J.P. Longtin, J. Appl. Phys. 91 (2002) 2530.
[24] K. Sokolowski-Tinten, D. von der Linde, Phys. Rev. B 61 (2000) 2643.
[25] H.Y. Sun, T.Q. Jia, Z.C. Wei, X.X. Li, C.B. Li, S.Z. Xu, D.H. Feng, H.Z. Wang, Z.Z. Xu, Opt. Mater. 28 (2006) 1372.
[26] X.C. Wang, G.C. Lim, H.Y. Zheng, F.L. Ng, W. Liu, S.J. Chua, Appl. Surf. Sci. 228 (2004) 221.
[27] J.L. Oudar, D. Hulin, A. Migus, A. Antonetti, F. Alexandre, Phys. Rev. Lett. 55 (1985) 2074.
[28] J. Shah, R.F. Leheny, C. Lin, Solid State Commun. 18 (1976) 1035.
[29] S.Z. Xu, T.Q. Jia, H.Y. Sun, C.B. Li, X.X. Li, D.H. Feng, J.R. Qiu, Z.Z. Xu, Optics Commun. 259 (2006) 274.
[30] S.Z. Xu, T.Q. Jia, X.X. Li, D.H. Feng, H.Y. Sun, C.B. Li, X.F. Wang, H. Kutoda, R.X. Li, Z.Z. Xu, Japan. J. Appl. Phys. 44 (2005) 8201.